 DOI: 10.1002/masy.200650817

Siloxane-containing Bifunctional Epoxide Together with Multi-functional Acrylates to Improve the Performance of Holographic Gratings

Yusuke Kawakami, Yeong Hee Cho*

Summary: Well-defined transmission holographic gratings with high diffraction efficiency were fabricated by irradiating a mixture of dipentaerythritol penta-/hexa-functional acrylates, 1-vinyl-2-pyrrolidone and 1,3-bis(3-glycidoxypropyl)-1,1,3,3-tetramethyldisiloxane or 1,3-bis[2-(1,2-epoxycyclohex-4-yl)ethyl]-1,1,3,3-tetramethyldisiloxane in the absence (photo-polymer systems, 30 : 10 : 60 in weight ratio; 80 or 55% efficiency) or presence (holographic polymer dispersed liquid crystal systems: 45 : 9 : 36 : 10 in weight ratio; 83 or 67% efficiency) of commercial liquid crystalline compound E7 with diphenyliodonium hexafluorophosphate and 3,3′-carbonylbis(7-diethylaminocoumarin) photo-initiating system by Nd:YAG laser ($\lambda = 532$ nm). When the ratio of dipentaerythritol penta-/hexaacrylate and 1,3-bis(3-glycidoxypropyl)-1,1,3,3-tetramethyldisiloxane was changed to 50 : 40 in photo-polymer system, the diffraction efficiency increased to 84%. They had smooth surface morphologies with regulated spacing. In polymer dispersed liquid crystal system, the same ratio of dipentaerythritol penta-/hexaacrylate and siloxane-containing epoxides gave the best results. 1,5-Bis(3-glycidoxypropyl)-1,1,3,3,5,5-hexamethyltrisiloxane and 1,5-bis[2-(1,2-epoxycyclohex-4-yl)ethyl]-1,1,3,3,5,5-hexamethyltrisiloxane gave high diffraction efficiency with 10% E7 (97% and 75%). The trisiloxane derivatives gave gratings with considerably or moderately reduced angular deviation (0.83, 0.66 degree for trisiloxane from 1.2, 0.7 degree for disiloxane derivatives, respectively for signal beam, and 0.76, 0.70 degree from 1.1, 1.0 degree for the reference beam at 32 degree of external incident angle) from Bragg profile, namely 5.2 and 4.5% volume shrinkage for trisiloxane, and 7.5, 5.6% for disiloxane derivatives, respectively. Gratings with diffraction efficiency over 95% with the narrowest angular selectivity of 4.0 degree was obtained when trimethylolpropane triacrylate was used together with 1,5-bis[2-(1,2-epoxycyclohex-4-yl)ethyl]-1,1,3,3,5,5-hexamethyltri-siloxane (50 : 40) and 5% E7. These gratings were actually used to store real images.

Keywords: cationic ring-opening polymerization; diffraction efficiency; holographic gratings; holographic polymer dispersed liquid crystal; modulation of refractive index; multi-functional acrylate; phase separation; photo-polymer; radical polymerization; siloxane-containing epoxide

1. Introduction

Optical holography[1,2] recording promises storage density and rate of data transfer which far exceed those of traditional magnetic and optical recording. There are basically two types of recording systems, namely photo-polymer and holographic polymer dispersed liquid crystal systems. In actual fabrication, dry film, [3,4] solution, [5,6] and liquid crystal (LC) composite types are used. [7,8]

Kawabata[9] developed a photo-polymer system consisting of a radically polymeriz-

School of Materials Science, Japan Advanced Institute of Science and Technology (JAIST), Asahidai 1-1, Nomi, Ishikawa, 923-1292 Japan
Tel.: +81-761-51-1630; fax: +81-761-51-1635.
E-mail: kawakami@jaist.ac.jp

able monomer (RPM) and a cationically polymerizable monomer (CPM) to write reflection holograms.

In holographic polymer dispersed liquid crystal (HPDLC) systems, LC phase-separated into sub micrometer size, in contrast to polymer dispersed liquid crystal system having micrometer size LC droplets. [10,11] The performance of the gratings strongly depends on the final morphologies, sizes, distribution, and shapes of LC domains. The size can be controlled by adjusting the kinetics of polymerization and phase separation of LC during the polymerization. R.L. Sutherland[12,13] created the switchable holograms by combining LC with multi-functional acrylates and explored the electro-optical effects. High diffraction efficiency approaching 100% was obtained, and the Bragg gratings showed a very narrow angular selectivity ($<1^\circ$).

Multi-functional acrylates such as DuPont's HRF[14,15] and Polaroid's DMP-128[16] have been most widely used as radically polymerizable cross-linking compounds, but they have some drawbacks such as volume shrinkage and multi-step processing. Success in further development of holography for various applications depends on the creation of hologram gratings with high resolution and sharp angle selectivity by properly designing the characteristics of the materials used.

We have focused on compounds with silicon-oxygen bonds as holographic recording materials. Actually, silicon-containing epoxide was found effective to induce efficient separation of LC from polymer matrix, and to realize high diffraction efficiency and low volume shrink age HPDLC system[17]. Siloxane component in CPM was expected to induce its efficient separation into dark regions from polymer matrix formed by RPM at the position of light interference. Large modulation of refractive index was anticipated due to their incompatibility and difference in refractive index compared with carbon-based matrix materials.

2. Experimental

2.1 Materials for Holographic Recording

Tri(propylene glycol) diacrylate (**2F,** $n_D^{20} = 1.450$), trimethylolpropane triacrylate (**3F,** $n_D^{20} = 1.474$) and dipentaerythritol penta-/hexaacrylate (**5F,** $n_D^{20} = 1.495$) were used as radically polymerizable cross-linking multifunctional acrylates (MFA). 1-Vinyl-2-pyrrolidone (**NVP,** $n_D^{20} = 1.512$) was used as a radically polymerizable reactive diluent. Structures of ring-opening cross-linkable compounds as cationically ring-opening polymerizable reactive diluent are shown in Figure 1.

Carbon-based epoxides were commercial products from Aldrich. Siloxane based epoxides were synthesized by hydrosilylation of allyl glycidyl ether and 3-vinylcyclohexene oxide with 1,3- or 1,5-dihydrosilanes.[17f] All products gave reasonable NMR signals. A commercial LC, **E7** (mixture of cyano bi-/terphenyls with high birefringence; $n_o = 1.5216$, $n_e = 1.7246$, and adequate T_{NI} (nematic-isotropic transition temperature : 61°C) was used.

Diphenyliodonium hexafluorophosphate and 3, 3′-carbonylbis(7-diethylaminocoumarin) (0.3 - 3wt%, 0.1 – 0.3wt % in the recording solution) were selected as PI and PS. The recording solution was composed of a fast-curing MFA, reactive diluent NVP and CPM in the ratio of 30–50, 8–10, and 32–60 wt%, in the absence or presence (5–20 wt%) of E7.

2.2 Formation and Characterization of Transmission Holographic Gratings

The optical set up of the laser system is illustrated in Figure 2.

Recording solutions were injected into a glass cell with a gap of 20 μm controlled by bead spacer. Nd:YAG solid-state continuous wave laser (Coherent lnc., Verdi-V2) with 532 nm wavelength and power 0.8–10 mW/cm^2 was used as the irradiation source.[17] The beam was split by controlling the two λ/2 plates and polarizing beam splitter. The separated two *s*-polarized beams with equal intensities were reflected by two mirrors and irradiated to recording

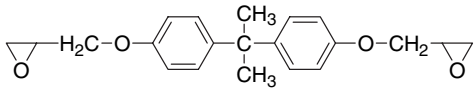

Bisphenol A diglycidy lether (**A**)

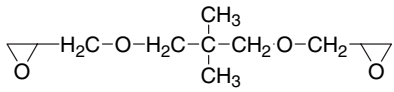

Neopentylglycol diglycidyl ether (**B**)

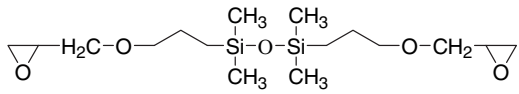

1,3-Bis(3-glycidoxypropyl)-1,1,3,3-tetramethyldisiloxane (**C**)

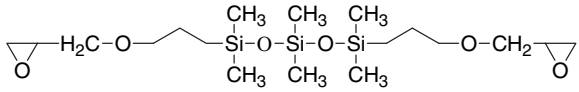

1,3-Bis(3-glycidoxypropyl)-1,1,3,3,5,5-hexamethyltrisiloxane (**D**)

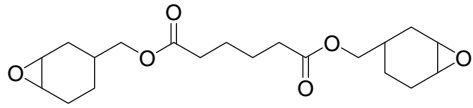

Bis[(1,2-epoxycyclohex-4-yl)methyl] adipate (**F**)

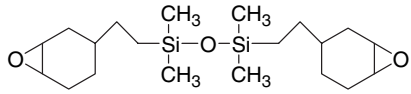

1,3-Bis[2-(1,2-epoxycyclohex-4-yl)ethyl]-1,1,3,3-tetramethyldisiloxane (**G**)

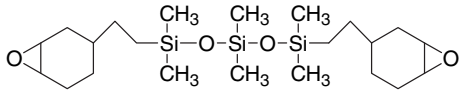

1,5-Bis[2-(1,2-epoxycyclohex-4-yl)ethyl]-1,1,3,3,5,5-hexamethyltrisiloxane (**H**)

Figure 1.
Chemical structures of ring-opening cross-linkable monomers.

solution at a pre-determined angle (2θ). The incident beam angle was varied from 16 to 40° (θ).

Diffraction efficiency is defined as the ratio of diffraction intensity after recording (I_d) to transmitted beam intensity before recording (I_t) as illustrated in Figure 3.

Real-time diffraction efficiency was measured by monitoring the intensity of diffracted beam when the shutter was closed at a constant time interval during the hologram recording. Samples for surface morphology observation were prepared by freeze-fracturing and washing with methanol, and examined with atomic force microscopy (AFM, JEOL JSPM-4210) in tapping mode and scanning electron microscope (SEM, Hitachi S-4100 with E-1030 ion sputter).

3. Results and Discussion

3.1 Photo-polymer System

3.1.1 Performance of Holographic Gratings

For simple nonslanted transmission gratings, maximum diffraction efficiency

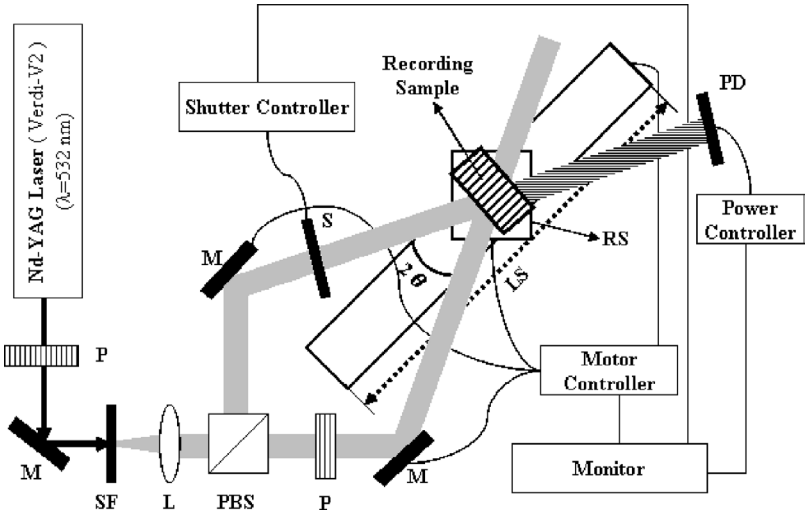

Figure 2.
Experimental setup for the holographic recording and real-time reading; P: 1/2λ plate, M: mirror, SF: spatial filter, L: collimating lens, PBS: polarizing beam splitter, S: shutter, LS: linear stage, RS: rotation stage, PD: power detector.

is given by Kogelnik's coupled wave theory[18]:

$$\eta = \sin^2[\pi \Delta n T/\lambda \cos\theta]$$

where η is the maximum diffraction efficiency, Δn is the modulation of refractive index of the medium after recording, T is the thickness of the hologram, λ is the recording wavelength, and θ is the half-angle of internal incident beams. T, λ and the external θ were fixed as 20 μm, 532 nm, and 16°, the actual internal incident beam angles were about 10° calculated by Snell's law[19]. Under these conditions, diffraction efficiency was basically controlled by Δn. Refractive index, viscosity, contrast of refractive index, Δn, and maximum diffraction efficiency of the formed gratings for all the CPM are summarized in Table 1.

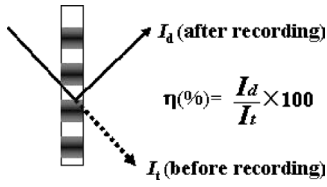

Figure 3.
Diffraction efficiency.

Diffraction efficiency of the grating with **5F**, **NVP**, and CPM was shown in Figure 4.

In the grating formation, diffraction efficeincy is controlled by the refractive index modulation (determined by refractive index contrast) and the extent of the phase separation of the components. In the present study, diffraction efficiency of diglycidyl ether derivatives increased in the order of **A** < **B** < **C**, although contrast of refractive index increased in the order of **B** < **C** < **A**. Phase separation controlled by diffusion of the components seems to play an essential role. It may be considered that in the polymerization, **5F:NVP:CPM(A),** diffusion of **A** to low intensity fringes was suppressed due to its high viscosity. Diffusion of **5F** from low intencity fringes to high-intensity fringes was also suppressed. They were trapped in a highly cross-linked region and will not contribute to high Δn. **B,** having a lower molecular weight and a more flexible structure, induced higher diffraction efficiency than **A**. In the case of **C** having siloxane chain, much higher diffraction efficiency was obtained. **C** seemed to easily diffuse to lower intensity fringes due to its flexible and incompatible properties. The flexible chain also helped

Table 1.
Refractive Index and Viscosity of CPM, and Maximum Diffraction Efficiency and Generated Δn of the Formed Gratings[a]

Structure	Refractive index (n_D^{20}, [b])	Viscosity (Cst, 25°C)	Contrast of refractive index to RPM ($n_{av.}$[c] = 1.495)	Modulation of refractive index (Δn)[d]	Diffraction efficiency (%)
A	1.586	3450 [e]	0.091	0.00517	34
B	1.457	31	0.038	0.00751	62
C	1.452	9	0.043	0.00922	80
F	1.493	664	0.002	0.00483	30
G	1.481	40	0.014	0.00693	55
H	1.474	42 ~ 45	0.021	0.00754	62

[a] **5F**: NVP : CPM (A – H) = 30 : 10: 60 (wt%).
[b] Refractive index, n_D^{20}, was measured by refractometer (DRM 3000, Otsuka Electronics Co., Ltd.).
[c] $n_{av.}$: average of refractive index of RPM.
[d] Modulation of refractive index, Δn, was calculated by Kogelnik's equation, and the actual internal incident beam angles were calculated by Snell's law.
[e] ow Plastics.

the further diffusion of remaining **5F** and **C** to high and low intensity fringes, respectively.

Compound **F** had the lowest diffraction efficiency due to its lowest contrast of refractive index and higher viscosity. Compound **G** and **H** showed 55 and 62% diffraction efficiency, which were lower than that of **C**, probably because **H** has higher molecular weight with more bulky cyclohexene oxide functional group and lower diffusibility than **C**.

As shown in Figure 4, induction period of grating formation was the least for **A** because of its highest viscosity, and for **C** was the maximum because of its flexible nature. The induction period of grating formation increased in the order of **F** < **H** < **G**, which was consistent with the above discussion.

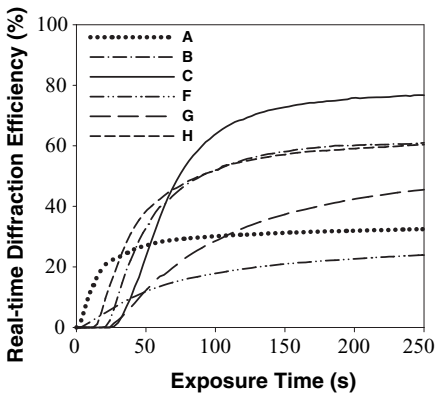

Figure 4.
Real-time diffraction efficiency of the gratings formed at a constant concentration of 1 wt% PI and 0.1 wt% PS, and at 40 mW/cm^2 intensity with **5F** : **NVP** : CPM (**A** – **H**) = 30 : 10 : 60 (wt%).

3.1.2 Effects of the Ratio of 5F and CPM on Real-time Diffraction Efficiency

The ratio of **5F** and CPM plays an important role in forming the gratings with high diffraction efficiency, since the polymerization rate and cross-linking density depend on the concentration of **5F**. To improve the diffraction efficiency of the **5F**-**G** (diffraction efficiency; 55%), the ratio of **5F** : **G** was varied from 30 : 60 to 70 : 20 (wt %) at constant concentration of 10 wt % **NVP**, and the results were shown in Figure 5.

By increasing the concentration of **5F** from 30 to 50 wt%, the final diffraction efficiency increased from 55 to 84% and decreased to 38% by further increasing the concentration to 70 wt%. When the concentration of **5F** is too high, gelation of the recording solution occured in very short time trapping **5F** and **G** in highly cross-linked region, and resulted in the decrease of the final diffraction efficiency. The slight decrease in diffraction efficiency during the exposure might be attributed to the initial

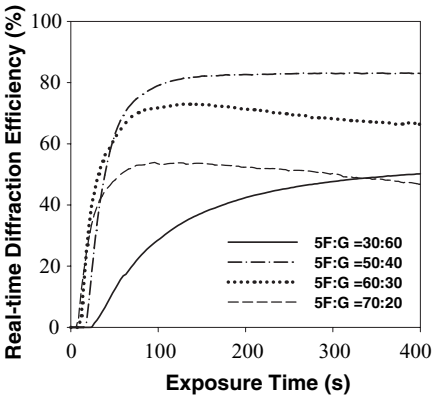

Figure 5.
Effects of ratio of **5F** and **G** on real-time diffraction efficiency of the gratings at the ratios of **5F**:**G** from 30 : 60 to 70 : 20 (wt %) and at 40 mW/cm^2 intensity with 1 wt% PI and 0.1 wt% PS.

fast nonequibrium cross-linking followed by the relaxation of the structure.

3.1.3 Surface Topology of the Gratings

The grating of high diffraction efficiency over 80% formed with **C** had clear and smooth surface than those with G at the same 5F : NVP : CPM ratio.

However, it is worthwhile to comment that the smoothness of the grating surface is not directly related to the diffraction efficiency, since refractive index modulation determines the diffraction efficiency. Well-defined structure of the gratings was also evidenced by SEM. Clearly layered structures were observed not only in surface view but also in cross-sectional view. Even partly fractured cross-sectional layeres slipped out from the inner layered structure can be seen in the surface view. Apparently, in the lowest intensity regions of interference, only slight or no cross-linking occured by the polymerization of RPM or CPM, although, this is undesirable from the viewpoint of stability.

3.1.4 Storage of Real Image of Screw

Real images of a screw were successfully stored using **C** and captured by CCD camera, which showed a very clear and stable image when only the reference beam was irradiated into the sample, as shown in Figure 7.

3.2 Polymer Dispersed Liquid Crystal System

3.2.1 Effects of Siloxane-containing bis(epoxide)s on the Performance of Gratings

Figure 8 shows the effects of chemical structures of bisepoxides on real-time diffraction efficiency at constant concentration of E7 (10 wt%) in recording solution [5F : NVP : (A – H) = 50 : 10 : 40 relative wt %].

In the grating formation by the phase separation of liquid crystalline **E7** from polymer matrix components, siloxane segments play an essential role to obtain high diffraction efficiency. As expected, gratings

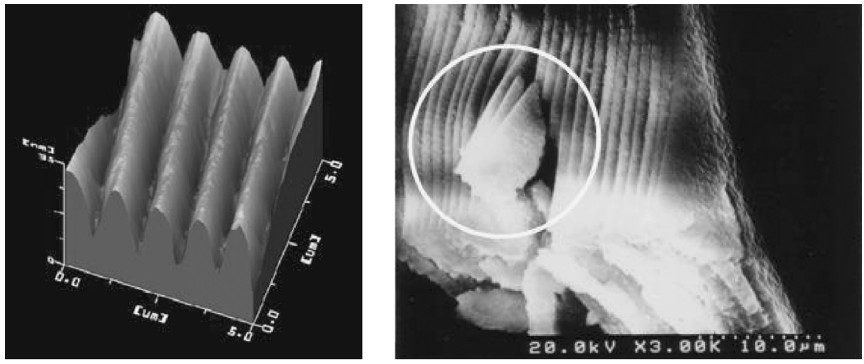

a) b)

Figure 6.
Surface morphology of transmission holographic gratings formed with **C** as CPM: (a) AFM and (b) SEM.

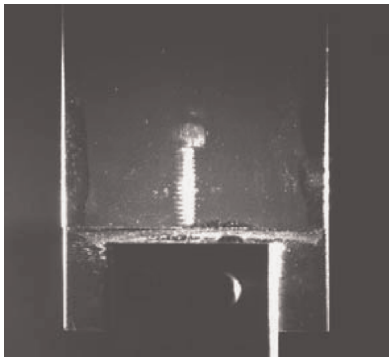

Figure 7.
Real image of a screw recorded in photopolymerizable material with **C** as CPM.

formed with **C** had remarkably higher diffraction efficiency than those formed with **A** and **B** without siloxane component, which seemed to have resulted from the good phase separation of **E7** from polymer matrix toward low intensity fringes because of its easy diffusion through the siloxane segments. The diffraction efficiency gradually increased and reached to higher value, which resulted from the further phase separation of **E7**. The highest diffraction efficiency 97% was observed for **D** with trisiloxane chain. Gratings formed with **G** and **H** having siloxane component also had higher diffraction efficiency than **F** without it. However, compared with **C** and **D**, **G** and **H** did not give higher diffraction efficiency. **G** and **H** have bulkier cyclohexene oxide as functional group, have higher viscosity, and form hard matrix, accordingly the diffusion of **E7** toward low intensity fringes seems difficult compared with the cases using **C**or **D**.

3.2.2 Volume Shrinkage of the Gratings Depending on the Structure of bis(epoxide)

Photo-polymerizable system as holographic recording material usually causes significant volume shrinkage during the formation of gratings, which can distort the recorded fringe pattern and cause angular deviations in the Bragg profile. For the measurement of volume shrinkage, slanted holographic gratings were fabricated by simply changing the angles of reference (R) and signal (S) beams, as shown in Figure 9.[20]

R and S are recording reference (0°) and signal (32°) beams. φ (16° in this study) is the slanted angle. Solid line in the grating indicates the expected grating. d is the sample thickness. Actual grating formed by S and R was deviated from the expected grating shown by dashed line by volume shrinkage of the grating. Presumed signal

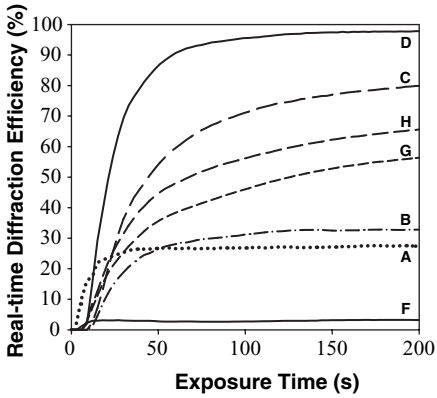

Figure 8.
Real-time diffraction efficiency of the gratings formed with (**A** – **H**) with 10 wt % **E7** [**5F**: **NVP**: (**A** – **H**) = 50: 10: 40 relative wt %].

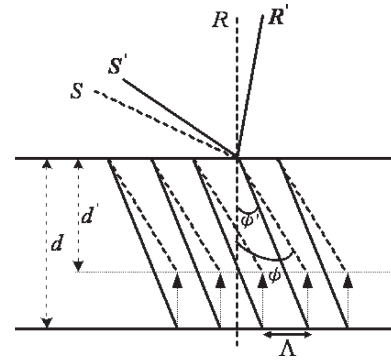

Figure 9.
Fringe-plane rotation model for slanted transmission holographic recording to measure the volume shrinkage.

beam (S′), which should have given actual grating was detected by rotating the recorded sample with reference light R off. R′ and S′ are presumed compensation recording reference and signal beams. φ' is the slanted angle in presumed recording with S′ and R′, and d' is the decreased sample thickness caused by volume shrink-

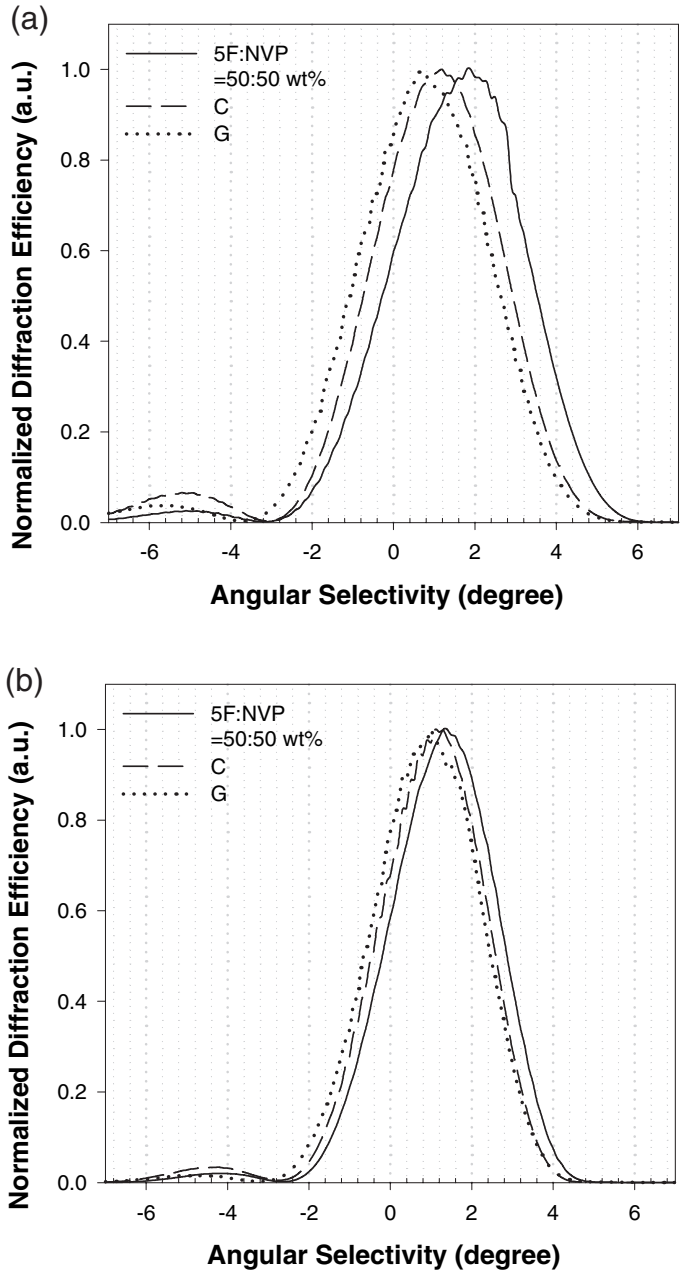

Figure 10.
Angular deviation from the Bragg profile for the gratings formed with **C** and **G** [**5F**: **NVP** : (**C** or **G**) = 50: 10: 40 relative wt %] detected by (a) diffracted S beam, and (b) diffracted R beam.

age. Degree of volume shrinkage can be calculated by following equation;

$$\text{Degree of volume shrinkage} = 1 - \frac{d'}{d}$$
$$= 1 - \frac{\tan\varphi'}{\tan\varphi}\left(\tan\varphi' = \frac{\Lambda}{d},\ \tan\varphi = \frac{\Lambda}{d'}\right)$$

Figure 10 shows the angular deviations from the Bragg profile of the gratings formed with **C** and **G**, respectively, at constant concentration of **E7** (10 wt%). The diffraction efficiency after overnight was only slightly changed, which indicated negligible volume shrinkage. Diffraction efficiency, angular deviation, and volume shrinkage of each system were summarized in Table 2.

As anticipated the gratings formed with only radically polymerizable multi-functional acrylate (**5F** : **NVP** = 50 : 50 relative wt%) showed the largest angle deviation, and the largest volume shrinkage of 10.3%. Such volume shrinkage could be reduced by combining the ring-opening cross-linkable monomers such as bis(cyclohexene oxide)s which are observed to reduce the volume shrinkage (5.6%). One of the possible reasons for small volume shrinkage is the effective formation of IPN structure, on which the work is in progress.

3.2.3 Optimization of Conditions to form Gratings with high Diffraction Efficiency and low Volume Shrinkage

Since the gratings formed with bis(cyclohexene oxide) showed only smaller volume shrinkage, optimization was carried out to create the gratings with low volume shrinkage and high diffraction efficiency. Changes in diffraction efficiency of the gratings formed with recording solutions consisting of **NVP** and **5F**, **3F**, and **2F** as MFA were studied at constant concentration of **E7** (10 wt%) [MFA : **NVP** : **H** = 50 : 10 : 40 relative wt%]. High diffraction efficiency over 85% was observed for **3F** and **H**. In case of **5F**, curing process seems to be too fast, contrary, in case of **2F**, cross-linking density seems to be too low to push **E7** out toward the low intensity fringes.

Figure 11 shows the change in diffraction efficiency of gratings formed with **H** and **3F** with the various concentration of **E7** [**3F**: NVP: **H** = 50: 10: 40 relative wt%].

Maximum diffraction efficiency over 95% was obtained in gratings formed with 5 wt% **E7**. With increasing **E7** concentration from 5 to 20 wt%, diffraction efficiency decreased gradually. Excess of phase separation, caused by too high loadings, will lead to the collapse of the gratings.

3.2.4 Angular Selectivity

When the multiplex hologram recording is required, it is necessary to realize sharp angular selectivity. The smaller the angular deviation, the more multiplex data or gratings can be recorded. [21,22] Angular selectivity ($\Delta\theta_{ang}$) is defined by Kogelnik's coupled wave theory as follows:

$$\Delta\theta_{ang} = \frac{1}{2n\sin\theta}\sqrt{\left[\left(\frac{\lambda}{T}\right)^2 - \left(\frac{\Delta n}{\cos\theta}\right)^2\right]}$$

where n is the average refractive index of recording solution, θ is the internal incident beam angle, T is the thickness of the hologram, λ is the recording wavelength, and Δn is the modulation of refractive index of solution after recording.

Table 2.
Deviations from Bragg angle of diffracted S and R beams (degree) and degree of volume shrinkage and diffraction efficiency determined by S beam[a] at recording solution of **5F** : **NVP** : **CPM** (**C**, **G**, **D**, and **H**) = 50: 10: 40 wt %, of **5F** : **NVP** = 50 : 50 wt%

Recording solution	Diffraction efficiency (%)[a]	Angular deviation of diffracted		φ'	Degree of volume shrinkage (%)
		S beam (degree)	R beam (degree)		
5F: NVP = 50:50 wt %	2	1.8	1.35	14.42	10.3
C	47	1.2	1.1	14.85	7.5
G	29	0.7	1.0	15.15	5.6
D	54	0.83	0.76	15.21	5.2
H	31	0.66	0.70	15.32	4.5

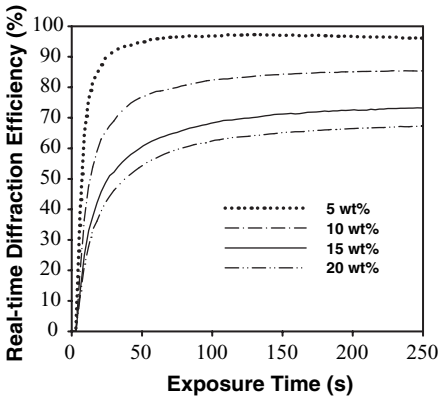

Figure 11.
Real-time diffraction efficiency of the gratings formed with **H** and **3F** and various concentration of **E7** [**3F**: **NVP**: **H** = 50: 10: 40 relative wt %].

Angular selectivities of our samples were similar, irrespective of the structures of epoxides (about 4°) as typically shown in Figure 12. Solid line represents the simulated theory values according to the Kogelnik's coupled wave theory.

Our experimental data showed only a little deviation from the theoretical values, which might be attributed to the slight reduction in thickness by small volume shrinkage. Adjustment of inter beam angle is also carried out to further reduce the angular selectivity. By increasing the incident beam angle, angular selectivity could be reduced to 2° even though their diffraction efficiency was little decreased.

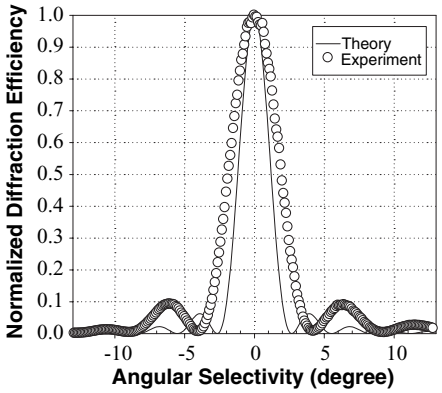

Figure 12.
Angular selectivity of gratings formed with **H**, **3F**, and 5 wt % **E7** [**3F**: **NVP** : **H** = 50: 10: 40 relative wt %] at external inter beam angle of 32 degree.

4. Conclusion

We have demonstrated the effectiveness of the introduction of siloxane component to ring opening cross-linkable reactive diluent to enhance the performance of holographic gratings. In the photo-polymer system, diffraction efficiency of the gratings prepared with diglycidyl ether increased by the presence of siloxane segments in the compound, although the contrast of refractive index was lowered by the presence of siloxane segments. Phase separation controlled by diffusion of the components seemed to play an essential role. Diffusion of the components to low intencity fringes was suppressed by the higher viscosity of the compounds without siloxane segment. They were trapped in a highly cross-linked region and did not contribute to high modulation of refractive index. Compounds having siloxane chain seemed to easily diffuse to lower intensity fringes due to its flexible and incompatible properties. Although compounds with cyclohexane oxide function gave lower diffraction efficiency than glycidyl ether derivatives, the efficiency could be improved by selecting the proper concentration of the compounds, and real image could be stored.

In the polymer dispersed liquid crystal system, high diffraction efficiency over 97% was obtained by using 1,3-bis(3-glycidoxypropyl)-1,1,3,3,5,5-hexamethyltrisiloxane (**D**) and **E7** (10wt%). Gratings with much higher performance such as low volume shrinkage with 5.6% could be obtained in the case of 1,3-bis[2-(1,2-epoxycyclohex-4-yl)ethyl]-1,1,3,3-tetramethyldisiloxane (**G**). The lower diffraction efficiency (75%) and smaller angular selectivity (4°) with 1,5-bis[2-(1,2-epoxycyclohex-4-yl)ethyl]- 1, 1,3,3,5,5-hexamethyltrisiloxane (**H**) could be improved to 95% and 2°, respectively, by

varying the functionality of MFA, concentration of **E7**, and incident inter beam angles.

Acknowledgements: This work was partly supported by a Grant-in-Aid for Scientific Research (16205016) from the Ministry of Education, Science, Sports, Culture and Technology, Japan.

[1] J. F. Heanue, M. C. Bashaw, L. Hesselink, *Science* **1994**, *265*, 749.
[2] D. Psaltis, *Science* **2002**, *298*, 1359.
[3] S. Martin, C. A. Feely, V. Toal, *Appl. Opt.* **1997**, *36*, 5757.
[4] S. Calixto, *Appl. Opt.* **1987**, *26*, 3904.
[5] A. Fimia, N. Lopez, F. Mateos, R. Sastre, J. Pineda, F. Amat-Guerri, *Appl. Opt.* **1993**, *20*, 3706.
[6] R. Mallavia, F. Amat-Guerri, R. Shastre, *Macromolecules* **1994**, *27*, 2643.
[7] M. S. Park, B. K. Kim, J. C. Kim, *Polymer* **2003**, *44*, 1595.
[8] T. Kye, D. Nwabunma, *Macromolecules* **2001**, *34*(*26*), 9168.
[9] M. Kawabata, A. Sato, I. Sumiyoshi, T. Kubota, *Proc. SPIE* **1993**, *66*, 1914.
[10] T. J. Bunning, L. V. Natarajan, V. P. Tondiglia, R. L. Sutherland, *Annu. Rev. Mater. Sci.* **2000**, *30*, 83.
[11] D.E. Lucchetta, L. Criante, F. Simoni, *J. Appl. Phys.* **2003**, *93*(*12*), 9670.
[12] R. L. Sutherland, L. V. Natarajan, V. P. Tondiglia, T. J. Bunning, *Chem. Mater.* **1993**, *5*, 1533.
[13] R. T. Pogue, R. L. Sutherland, M. G. Schmitt, L. V. Natarajan, S. A. Siwecki, V. P. Tondiglia, T. J. Bunning, *Appl. Spectrosc.* **2000**, *54*(*1*), 12A.
[14] A. M. Weber, W. K. Smothers, T. J. Trout, D. J. Mickish, *Proc. SPIE-Int. Soc. Opt. Eng.* **1990**, *1212*, 30.
[15] W. J. Gambogi, A. M. Weber, T. J. Trout, *Proc. of SPIE-holographic imaging and materials*, **1993**, *2043*, 2.
[16] R. T. Ingwall, H. L. Fielding, *Opt. Eng.* **1985**, *24*, 808.
[17] a) Y. H. Cho, M. He, B. K. Kim, Y. Kawakami, *Science and Technology of Advanced Materials* **2004**, *5*, 319. b) Y. H. Cho, N. Kim, Y. Kawakami, *Proc. SPIE* **2004**, *5636*, 475. c) M. He, Y. H. Cho, N. Kim, Y. Kawakami, *Proc. SPIE* **2004**, *5636*, 560. d) M. He, Y. H. Cho, N. Kim, Y. Kawakami, *Design. Monom. Polym.* **2005**, *8*, 473. e) Y. H. Cho, R. Kawade, T. Kubota, Y. Kawakami, *Sci. Tech. Adv. Mater.* **2005**, *6*, 435. f) Y. H. Cho, C. W. Shin, N. Kim, B. K. Kim, Y. Kawakami, *Chem.Mater.* **2005**, *17*, 6263.
[18] H. Kogelnik, *Bell Syst. Tech. J.* **1969**, *48*, 2909.
[19] G. Pfaff, P. Reynders, *Chem Rev.* **1999**, *99*, 1963.
[20] D. A. Waldman, R. T. Ingwall, P. K. Dhal, M. G. Horner, E. S. Kolb, H.-Y. S. Li, R. A. Minns, H. G. Schild: *SPIE* **1995**, *2689*, 127.
[21] U. S. Rhee, H. J. Caulfield, J. Shamir, C. S. Vikram, M. M. Mirsalehi, *Opt. Engin.* **1993**, *32*(*8*), 1839.
[22] F. H. Mok, *Opt. Lett.* **1993**, *18*(*11*), 915.

